Physics of the Earth and Planetary Interiors 297 (2019) 106326

Contents lists available at ScienceDirect

Physics of the Earth and Planetary Interiors

journal homepage: www.elsevier.com/locate/pepi

Effects of Coulomb stress change on $M_w > 6$ earthquakes in the Caucasus region

Bahruz Ahadov[a,b], Shuanggen Jin[a,c,*]

[a] Shanghai Astronomical Observatory, Chinese Academy of Sciences, Shanghai 200030, China
[b] University of Chinese Academy of Sciences, Beijing 100049, China
[c] School of Remote Sensing and Geomatics Engineering, Nanjing University of Information Science and Technology, Nanjing 210044, China

ARTICLE INFO

Keywords:
Coulomb stress
Stress inversion
Seismicity rate
Caucasus

ABSTRACT

Coulomb stress variations may trigger earthquakes, while the stress transfer process is not clear. In this paper, Coulomb stress changes are investigated for the sequences of strong earthquakes in the Caucasus region, which followed the 1988 M_w6.8 in Spitak, the 1991 M_w6.9 in Racha and the 2000 M_w6.2 in Baku. Our results show that the mainshocks induced variations in the stress field where most of the seismic events occurred. Coulomb stress increases 2 bars corresponding nearly to places of aftershocks, while the stress falls above 10 bars for Racha mainshock. The calculated Coulomb stress loaded about 5 bars at the end of rupture plane and the stress falls ~9 bars for Spitak mainshock. Our stress pattern shows a correlation within the areas of Coulomb stress caused by the combination of seismicity. Correlations between the coseismic Coulomb stress changes and the observed spatial patterns of the aftershocks created by the mainshock are illustrated by the stress variations over both optimally oriented and specified fault planes. An apparent correlation between the mainshock stress changes and the detected spatial pattern of the aftershocks is found, confirming the utility of the stress maps in constraining the expected locations of the forthcoming aftershocks and mitigating earthquake hazards.

1. Introduction

Two destructive and large earthquakes occurred in the Caucasus, the M_w6.8 Spitak earthquake (December 7, 1988), which occurred on the Pampak-Sevan fault zone in Armenia and the M_w6.9 Racha earthquake in Georgia (April 29, 1991). Previous studies have shown that the rupture processes of these two large events were very complex and can be modelled with several sub-sources. The 1988 Spitak earthquake was the first instrumentally reported large event in Caucasus. The 1991 Racha earthquake was the largest instrumentally reported event in Caucasus. Although it was shallow and produced some landslides, there was not observed surface rupture. Catalogues of the historical seismicity in Caucasus showed that there were no earthquakes with a magnitude over 6, except the most destructive one, the 1668 Shamakhi earthquake, which affected the eastern half of the Greater Caucasus. These regions have been also characterized by intense and persistent volcanic activity. The magmatism in the mountain belt associated with the collision between the Eurasian and Arabian plates was started in late Miocene in the central part of the Caucasus. Recent plate tectonic models show that the Lesser and the Greater Caucasus are tectonically active with ongoing mountain building processes containing complex deformation with strain partitioning (Reilinger et al., 2006; Kadirov et al., 2014; Ahadov and Jin, 2017). In the principal region of the collision zone, most of the earthquakes occurred along active structure within the crust at the depth shallower than 40 km. The Caucasus is one of the seismically active regions due to the high probability of earthquake incident combined with high population extension, inadequate construction standards and lack of appropriate mitigation plans.

During the past decade, the phenomenon of static stress changes caused by an earlier earthquake can assist incoming earthquakes on nearby faults. Therefore, earthquake stress changes can be utilized in the interpretation of upcoming seismic hazards (Stein et al., 1997; Nalbant et al., 2002; Parsons, 2005). Moreover, evaluations of the stress variations following a mainshock might be used essentially an emergency response tool for mitigating hazards caused by the following aftershocks (Steacy et al., 2004; McCloskey and Nalbant, 2009). Coulomb stress changes are significant for earthquake interactions and seismic hazard evaluations. Several researchers have studied the stress change and the effects on major faults within 100 km of the Loma Prieta, California shock (Reasenberg and Simpson, 1992; Parsons et al., 1999). The Coulomb stress transfer model was applied to study the Landers and Northridge earthquakes (Hardebeck, 1998). Çakir et al.

* Corresponding author at: Shanghai Astronomical Observatory, Chinese Academy of Sciences, Shanghai 200030, China.
E-mail addresses: sgjin@shao.ac.cn, sg.jin@yahoo.com (S. Jin).

https://doi.org/10.1016/j.pepi.2019.106326
Received 27 January 2019; Received in revised form 4 October 2019; Accepted 7 October 2019
Available online 21 October 2019
0031-9201/

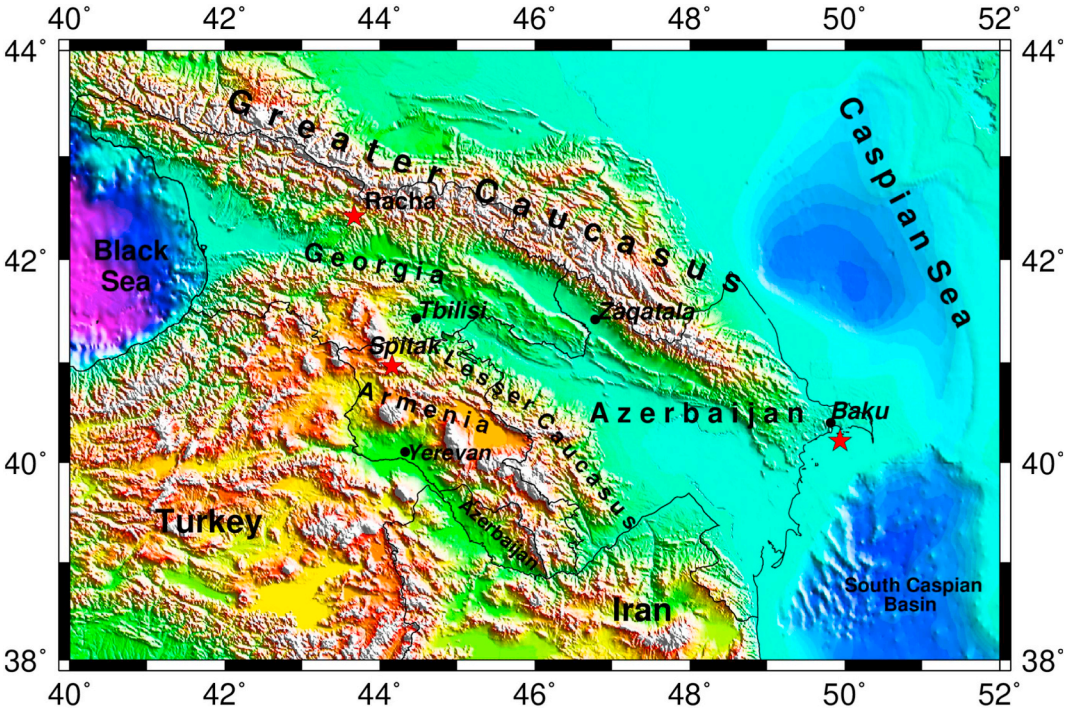

Fig. 1. Simplified topographic/bathymetric (SRTM30 PLUS) map of the study region and red stars show the location of the study cases. (For interpretation of the references to color in this figure legend, the reader is referred to the web version of this article.)

Table 1
Fault plane and focal parameters of the earthquake models.

Events	Date day/month/year	Lon (deg)	Lat (deg)	Depth (km)	Mw	Strike (deg)	Dip (deg)	Rake (deg)	Length (km)	Width (km)
Spitak	07/12/1988	44.16	40.96	6.3	6.8	307	60	159	45.5	14.4
Racha	29/04/1991	43.67	42.42	10	6.9	287	30	90	41.5	19.8
Baku	25/11/2000	49.94	40.22	33	6.2	318	85	−77	16.1	10.6

Table 2
Comparison of stress tensor inversion results for the sub-regions.

Regions	Data	σ_1(tr)	σ_1(pl)	σ_2(tr)	σ_2(pl)	σ_3(tr)	σ_3(pl)	Phi (R)
Spitak	19	3.1	5.2	102.8	62	270.4	27.5	0.79 ± 0.02
Racha	16	200.5	14	109	5.9	356.5	74.6	0.7 ± 0.08
Baku	10	169.6	75	73.6	1.6	343	14.8	0.59 ± 0.17

(2003) used the same method to investigate the 1999 İzmit and Düzce earthquakes in the Marmara region and deduced that İzmit and other events in this area triggered the Düzce earthquake. While a correlation between Coulomb stress changes and aftershock location has been reported often, several studies have questioned the validity of the Coulomb stress hypothesis and its predictive power. Toda and Stein (2003) stated a few cases that the Coulomb hypothesis predicts a reduction of seismicity in areas of negative Coulomb stress (stress shadows). Coulomb stress changes created by the mainshock are determined by computing the stress variations over both optimally oriented and specified fault planes, which may have a correlation between the stress changes of the mainshock and the observed spatial pattern of the aftershocks.

In this study, we aim to quantify the correlation between seismicity rate changes and modelled Coulomb stress changes for $M_w > 6$ earthquakes in the Caucasus region for the first time. The regional stress orientations and Coulomb stress are estimated on optimally oriented planes, which will provide a better understanding of stress state and seismic activity. In Section 2, regional tectonics setting is introduced, Coulomb failure and methods are shown in Section 3, results and discussion are presented in Section 4, and finally the conclusions are given in Section 5.

2. Tectonic setting

In the Caucasus region earlier studies have quantified regional deformation in the plate interaction zone (Reilinger et al., 2006; Ahadov and Jin, 2017). Eastern Turkey and Caucasus regions were observed with earthquake activity and high elevation (McKenzie, 1970). Regarding historical seismicity, massive earthquakes have occurred with magnitudes of $M_w > 6$ in the region. The Caucasus is one of the Earth's seismically active and deforming continental regions (Fig. 1).

The wide range of deformation processes makes it a unique place to understand the complexity of the continental collision in the region,

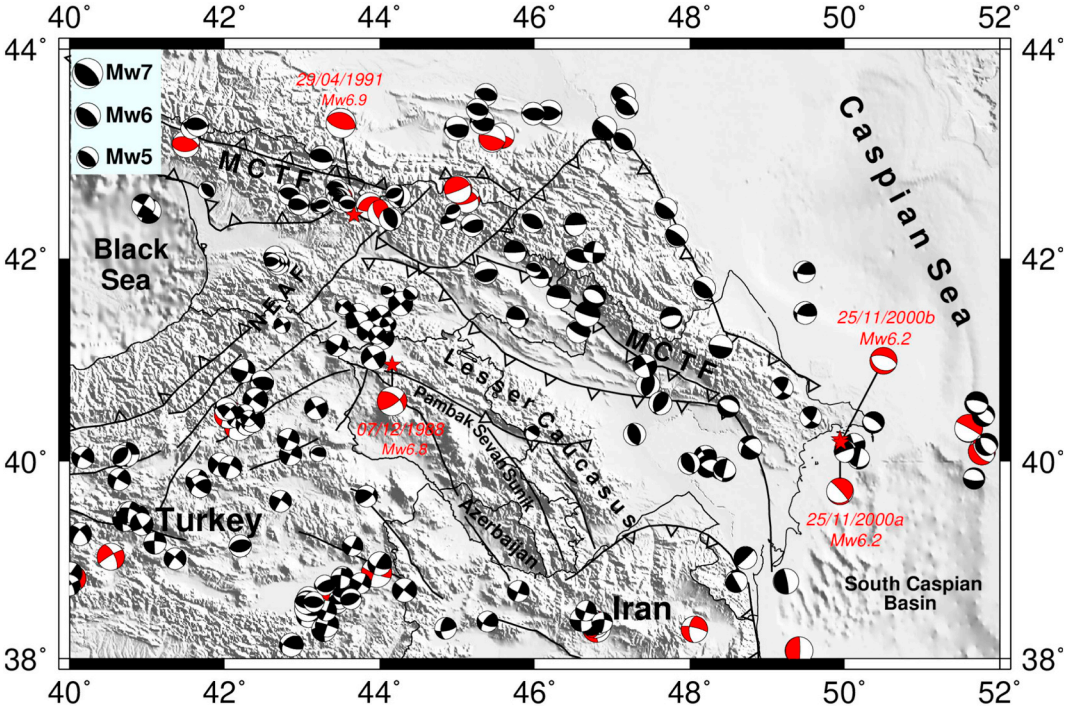

Fig. 2. Tectonic setting and seismicity indicated by the focal mechanisms of earthquakes, North East Anatolian Fault (NEAF) and Main Caucasus Thrust Fault (MCTF) (red color is indicate large earthquakes $M_w > 6$, 1976–2018). (For interpretation of the references to color in this figure legend, the reader is referred to the web version of this article.)

including strike-slip and thrust faulting. The south-eastern Anatolian and the Caucasus regions principally provide fold-belts along major thrust faults and strike-slip faults in the continental collision zone. The Eastern Greater Caucasus is located in the north of Azerbaijan which is known since the antiquity for its hydrocarbon resources and mud volcanoes. The Lesser Caucasus and the adjacent Anatolian present a predominance of strike-slip focal mechanisms joined with a system of vertical faults. In the Greater Caucasus, the convergence zone is adjusted by the reverse focal mechanism with a general N-S to NE-SW compression (Copley and Jackson, 2006; Barazangi et al., 2006; Tan and Taymaz, 2006).

The Caucasus region is distributed into three extensive tectonic units outlined by rigid and fold-thrust: Achara-Trialeti and the Greater Caucasus fold and thrust; the Kura and Rioni depressions; the northern Transcaucasian (Azerbaijan and Georgia). A zone with higher seismicity is observed on the southern slope west of Tbilisi (Georgia) in the Racha area of the Greater Caucasus (Triep et al., 1995). Studies of focal mechanisms and depths show that this seismicity is linked to several active fault strings in the subsurface of the Gagra-Dzhava zone. In the Absheron peninsula, focal mechanism solutions show thrust and normal faulting, and seismic activity by expanding the SSW-NNE to the east of the Greater Caucasus and the South Caspian Basin subduction zone. The seismicity confers a western segment of motion relative to Eurasia besides oriented thrusting towards the west as well as in the Gobustan desert area (Jackson et al., 2002; Allen et al., 2002). Armenia extends in the central part of the Armenian Highland and is located north of the border of the collision within the Arabian-Eurasian Plate. The right-lateral Pambak-Sevan-Sunik (PSS) is an active fault of the reverse component in Armenia (~400 km). The southern Javakhet upland is an active tectonic zone in the north part of Armenia.

3. Methodology

3.1. Coulomb failure

The Coulomb failure stress changes due to the mainshock are resolved onto the fault plane using earthquake parameters: location, length, width, slip, strike, dip and rake angles in the stress calculations. Places of probable future failure are then identified as increased Coulomb Stress effects.

$$\Delta\sigma_f = \Delta\tau - \mu'\Delta\sigma_n \quad (1)$$

where $\Delta\tau$ and $\Delta\sigma_n$ are the change in shear and normal stresses on likely future fault planes, respectively, while μ' is the apparent coefficient of friction with range 0–1. The limited stress can be related to fluid pore pressure by Skempton's coefficient, B, the rate of the change in pore pressure in a cavity to the difference in applied stress, where $\mu' = \mu(1 - B)$ (Roeloffs, 1988). The precision of the Coulomb stress changes depends on the accuracy of the source parameters and the receiver fault of the earthquake. Calculating the Coulomb failure fault for each nodal plane of focal mechanism solutions has been demonstrated to be useful to decrease the uncertainty of receiver faults in the different stress field (e.g., Toda, 2008; Ishibe et al., 2011, 2015). A reliable estimate of the slip distribution and fault geometry is therefore very important for stress transfer calculations. Small changes in fault geometry and slip distribution can contribute to serious perturbations in Coulomb failure stress especially nearby the sources region (King et al., 1994). Due to the lack of data availability, we could not calculate the Coulomb stress as source fault. We calculated the Coulomb stress changes from the focal mechanism solution of the earthquakes as receiver fault. The coseismic static stress changes following $M_w > 6$ earthquakes on the optimally oriented faults are calculated using

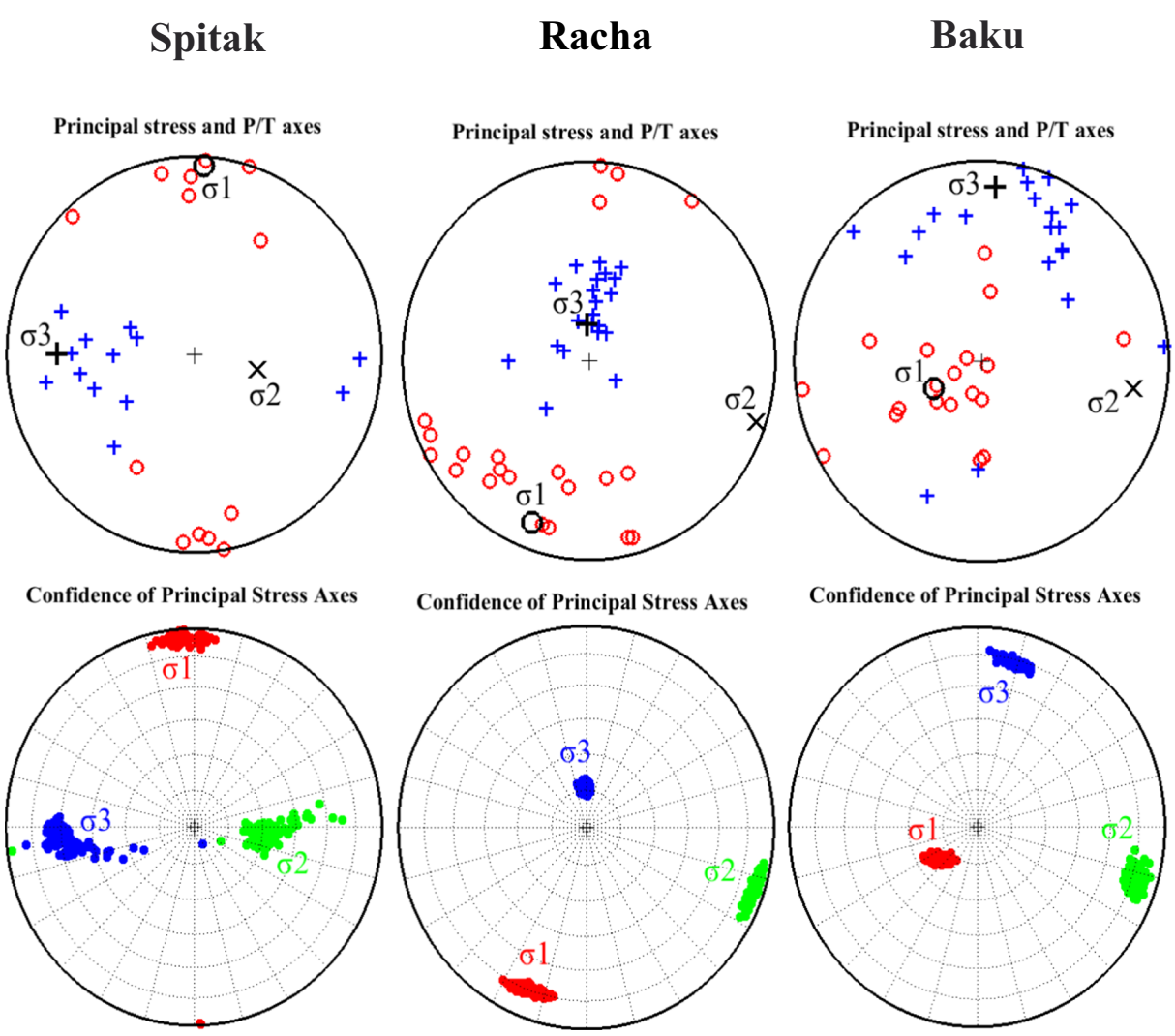

Fig. 3. Map represent P and T axis of the focal mechanisms. Small dots delineate the distribution of stress axis within the 95% confidence range. Azimuth (Az) and plunge (Pl) for each region is listed in Table 2.

Coulomb 3.4 software (Lin and Stein, 2004; Toda et al., 2005). The Earth was assumed as a homogeneous elastic half-space and faults were considered as rectangular dislocations embedded in it. In order to consider these assumptions in our calculation, Young modulus, shear modulus, Poisson ratio, and coefficient of friction were considered equal to 8×10^5 bars, 3.2×10^5 bars, 0.25, and 0.4 respectively. Detailed input parameters are given in Table 1.

We have examined the eligibility of results using various μ friction values (0.6 and 0.8). The spatial pattern of the Coulomb stress changes are not changed significantly contrasted to the results from 0.4 (Fig. S1).

Coseismic stress changes are most useful to correlate events close in time (0 to 10 years). When two events are widely separated in time instead of the post-seismic effects, because the relaxation of stresses in the lower crust and upper mantle can play an important role in the time-dependent redistribution of Coulomb stress. Knowledge of slip models, geometry of source faults and kinematics of receiver faults is needed for Coulomb stress modelling. These parameters can be obtained with reasonable details from recent, instrumentally-recorded earthquakes. We estimated the average slip for an earthquake using the empirical relationships from Wells and Coppersmith (1994) rupture length, width, and surface displacement.

3.2. Stress inversion

In addition, Coulomb stress changes are created by computing the stress variations over optimally oriented fault planes. The well-known methods of Gephart and Forsyth (1984) and Michael (1984) are proposed to determine the stress which minimizes the contrast between the resolved shear stress and the slip direction for each dataset. These algorithms describe the directions of three principal stress axes and the relative magnitudes of the stress axes $R = (\sigma_2 - \sigma_3)/(\sigma_1 - \sigma_3)$. Here σ_1,σ_2 and σ_3 indicates maximum, intermediate and minimum principal compressive stresses, respectively.

In this study, stress inversion is determined by the approach of Michael (1984) using a linear least-squares inversion technique. This algorithm uses both nodal planes to find the correct fault planes with determining the best stress tensor. The fundamental point of the

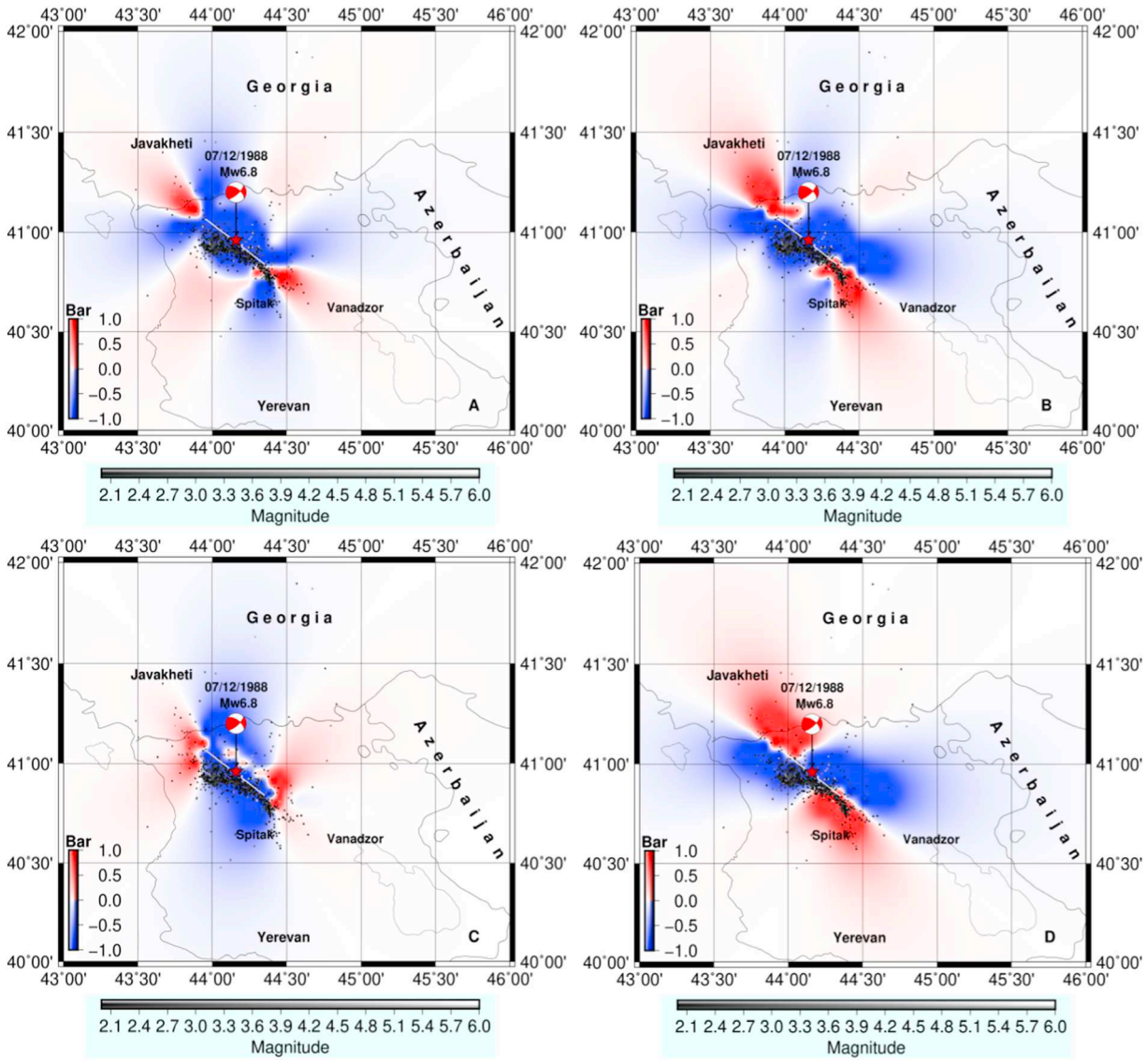

Fig. 4. Coulomb stress changes caused by the 1988 Spitak earthquake calculated over the specific receiver fault (A) strike 307°; dip 60°; rake 159° and optimally oriented (B) strike-slip faulting (C) thrust faulting and (D) normal faulting. The grey dots denote the epicenters of the $M \geq 2$ aftershocks from International Seismological Centre (ISC) between 1988/12/07–1990/12/07.

algorithm is the computation of the confidence limits of the principal stress axes directions. Confidence limits are calculated by a statistical tool known as bootstrap re-sampling.

4. Results and discussion

4.1. Local stress inversion

We have used Focal Mechanism Solutions (FMS) from different references, e.g., Tseng et al. (2016), Tan and Taymaz (2006) and Harvard CMT (Ekström et al., 2012) to study local stress variations (Fig. 2). To project changes in Coulomb stress onto optimal faults, it is necessary to estimate the orientation of the local stress field. Focal mechanism solution data is used for determining the directions and ratios of principal stress components in the area. The geographical distribution of focal mechanism solutions in the area is related to the distribution of active faults. Focal mechanisms are consistent with the overall sense of movements along faults and the study area is characterized by strike-slip and thrust faulting solutions.

The inversion results indicate that the maximum principal stress (σ1) is oriented in the SW-NE direction, minimum stress axes (σ3) is sub-horizontal striking in NE-SW direction and the intermediate principal stress (σ2) is trending vertical for the Racha region. The inversion results are estimated for the Spitak region and show that maximum principal stress (σ1) is sub-vertical striking in NE-SW direction, minimum stress axes (σ3) is trending horizontal, and the intermediate

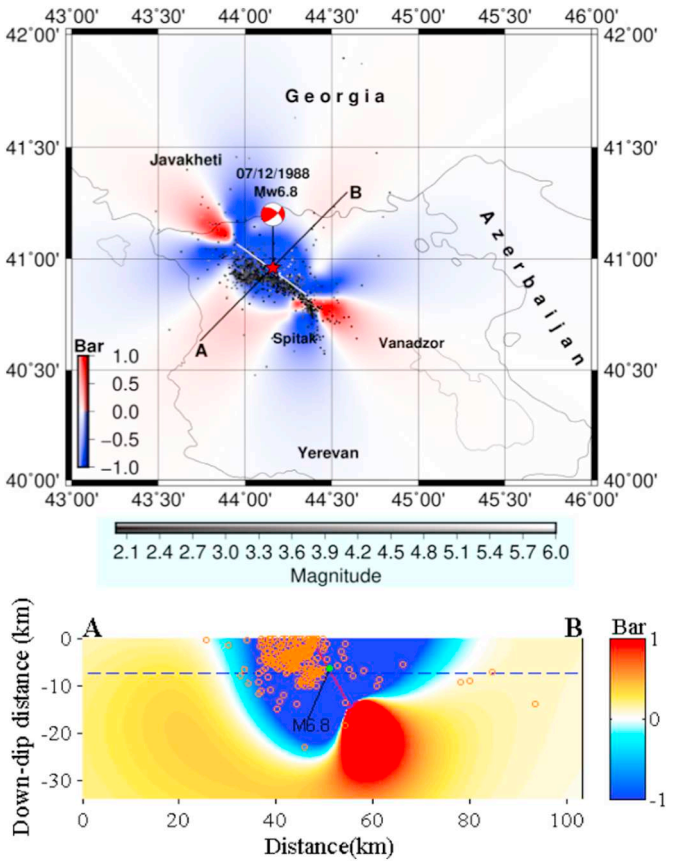

Fig. 5. Vertical cross-sections oriented perpendicular to the strike of the fault modelled during the 1988 Spitak earthquake along lines A-B.

principal stress (σ2) is vertical. While the stress for the Baku region shows that σ1 is sub-horizontal trending, σ2 is trending in the region SE-NW and σ3 is vertical in N-S direction (Fig. 3).

4.2. Spitak M_w6.8 earthquake in 1988

The Spitak Earthquake of 1988 December 7 is one of the destructive earthquakes in the last few decades. National Earthquake Information Center (NEIC) provided the source parameters as follows: location, 40.94°N, 44.29°E, and origin time, 07:41:24.9 UT. The origin of the Spitak Earthquake is located within the WNW-ESE orientated Pambak-Sevan fold and thrust belt in the south of the Lesser Caucasus. Pacheco et al. (1989) used broadband and long-period records to investigate the particulars of the causing process. They studied three subevents during the first 20 s and presented field measurements such as surface cracks and aftershock pattern. They found that the Spitak Earthquake had a strike-slip mechanism including a significant reverse-faulting component with source parameters: strike 307°, dip 60°, and rake 159°, depth 6.3 km.

Fig. 4 shows the Coulomb stress changes caused by the mainshock at a depth of 6.3 km. As shown in Fig. 4(A), the positive Coulomb stress areas generated by the Spitak earthquake are distributed in the north-west and NW-SE sides of the fault plane and the negative areas are in the north-south and west-east. The fault zones in the north-west and south-east of Spitak rupture are loaded by above 3 and 4 bars. However, the main of the fault plane is dropped to 8.6 bars. According to the distribution of Coulomb failure stress, we analyzed the relationship between aftershock location and stress change pattern. The northern part of the model generated a shadow zone with stress-reducing 0.5 bars. In Fig. 5, we present the Coulomb stress changes on a vertical cross-section (A-B) perpendicular to the fault strike of the event. The Coulomb stress distribution at 6.3 km depth computed on receiver faults with similar focal mechanisms of the mainshock. We observed a correlation between aftershocks and negative stress lobes except for four aftershocks.

Most of aftershocks are centered on the rupture plane, creating northeastward according to the temporal and spatial scattering of the aftershocks. Some aftershocks are clustered at the end of the rupture, where the stress rises. The existence of aftershocks is consistent with the rupture plane where the Coulomb stress is decreased on the nodal planes. About 80% of the events accumulate in the fields of negative stress changes in the north-west and the south-east parts of the rupture plane. The largest aftershock M_w5.9 has occurred in the north-east part of the Coulomb stress about 20 min later after the mainshock. Large aftershocks (5–5.9) happened in the negative area of Coulomb stress and while some moderate aftershocks are observed in positive stress. In Fig. 4(B) the stress changes are considered for optimum strike-slip faults, requiring a lobe of stress increase in the NW-SE, while the stress variations for thrusting faults (Fig. 4(C)) require a large lobe of stress shadow in the SE. The optimum strike-slip fault result is similar to main rupture stress orientation. When the stress changes resolved onto the optimum oriented thrust faults as shown in Fig. 4(C), it has seen that thrust faulting mechanisms fall into the areas of stress rise and the strike-slip mechanism fall into the areas of the stress decrease. From stress pattern resolved onto the optimum oriented normal faults as shown in Fig. 4(D), it has seen that there is approximately similar stress shadow of the optimum strike-slip faulting. As stated above, the stress changes appeared in Fig. 4(B, C and D) have been estimated using the regional stress field defined in this study.

4.3. Racha M_w6.9 earthquake in 1991

The Racha earthquake (M_w6.9) happened on April 29, 1991 in the southern part of the Greater Caucasus. It is stronger than the Spitak earthquake (M_w6.8) in 1988 and the biggest event ever reported in the region. The epicentral position of the Racha shock is located on the southern slope and near the main thrust of the Western Greater Caucasus (Fig. 2). The Lesser and Greater Caucasus are under a compressive stress regime, arising from the relative convergence of the Arabian plate with the Eurasian plate. The deformed region is defined by W-E striking thrust-folding and faulting (Philip et al., 1989).

Coulomb stress changes have been analyzed using accessible data related to the background and the receiver faults. Consistent area of Coulomb stress change describes the comparison of stress in the rupture areas, as well as the combination of secular stress and the drop of earthquake stress. Earthquakes usually relieve stress along with the ruptures, and typically transfer stress at some places beyond the rupture tips and off the fault (positive stress). The stress patterns in Fig. 6 have been imaged at a depth of 10 km. The stress changes due to the mainshock have been resolved onto the 1991 Racha M_w6.9 earthquake and optimally oriented rupture plane, as shown in Fig. 6(A, B, C and D). To investigate the transferred stress on the nearby faults, we calculated the

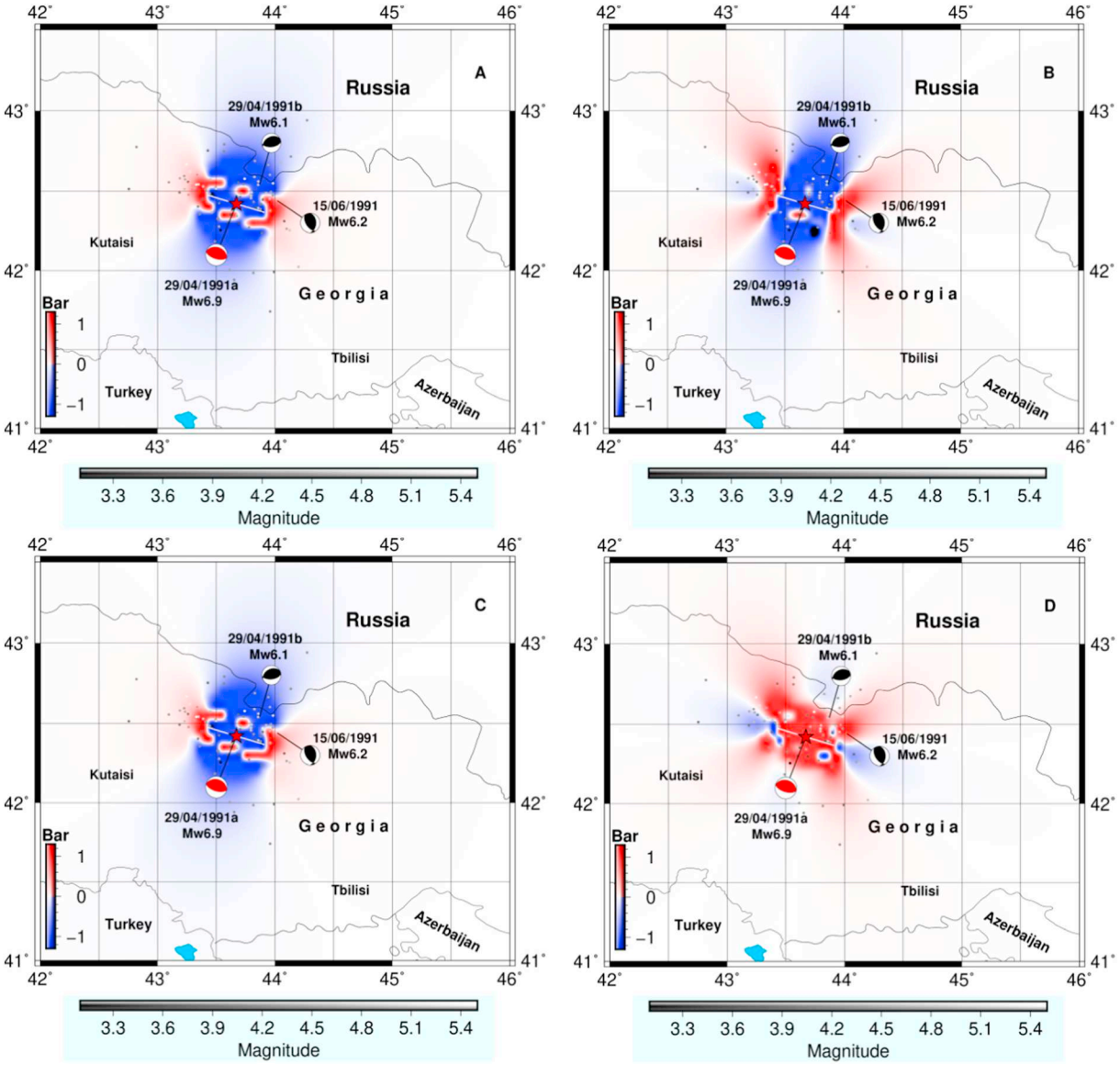

Fig. 6. Maps of Coulomb stress changes caused by the 1991 Racha earthquake calculated over the specific receiver fault (A) strike 287°; dip 30°; rake 90° and optimally oriented (B) strike-slip faulting (C) thrust faulting and (D) normal faulting. The grey dots denote the epicenters of the M ≥ 3.1 aftershocks (ISC, 1991/04/29–1993/04/29).

Coulomb stress changes following two events. Fig. 6(A) confers the decrease of Coulomb static stress in the northeast part where the second event is located. As a result, most of the largest aftershocks (5–5.5) location of the Racha 1991 earthquake, correlated with areas of decreased Coulomb stress changes following the mainshock. Majority of seismicity clustered near the ruptured plane (NW) where the variation is in the positive Coulomb stress values. We observed non-uniform accumulation of the aftershocks around the rupture plane. In this study, the geometry of the fault plane is assumed from the empirical relation from Wells and Coppersmith (1994). This might also be a reason for the more significant earthquakes, which affects the calculated fault geometry.

In Fig. 6, the stress differences have been resolved onto the optimally oriented mainshock (287°/30°/90°), strike-slip, thrust and normal faults using the regional stress field defined in this study. Fig. 6(A) shows that the Racha main rupture is partly stressed and partly under the stress shadow. Differences in stress indicate a lobed model of varying positive and negative stress changes around the rupture. The lobed patterns of Coulomb stress changes are calculated using regional stress direction (Table 1). A positive stress changes is dominated at end of the rupture and negative stress change observed in the northern and southern parts. In the case of strike-slip faulting orientation (Fig. 6(D)), most of the detected seismicity concentrates of positive stress change, except the earthquakes clusters at the end of the rupture zone with

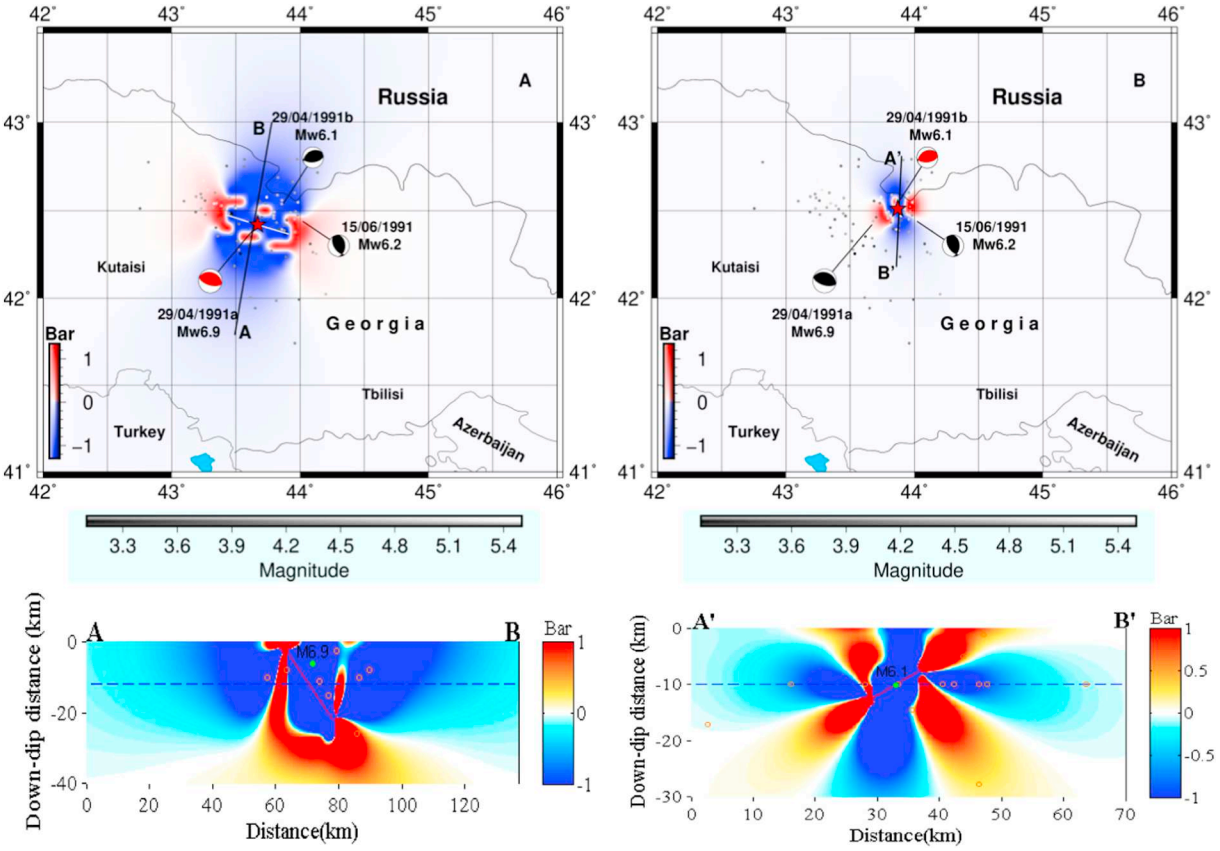

Fig. 7. Coulomb stress changes calculated for the first and second events. Vertical cross-sections oriented perpendicular to the strike of the fault modelled during the 1991 Racha earthquake along lines P1 (A′-A) and P2 (B′-B).

negative stress change.

The vertical cross-section confirms that the fault plane is associated with the first and second shocks (Fig. 7). We computed the static stress on a vertical cross-section perpendicular to the fault strike of the event. Coulomb stress decrease with different depths where aftershocks were located. The hypocenters fall in regions of negative stress changes and some hypocenters are located in positive stress changes.

4.4. Baku M_w6.2 earthquake in 2000

At the eastern end of the Greater Caucasus, a double-source event happened on November 25, 2000 (Fig. 2). The time delay of the second energy release was only ~90s, and both earthquakes had a similar energy release. Although their locations are very close, but the faulting mechanism is different. Tan and Taymaz (2006) found the source parameters of the first event of the Baku earthquakes to be as follows: strike 318°; dip 85°; rake −77° with WNW-ESE fault orientation and centroid depth is 40 km. Jackson et al., (2002) investigated almost similar source parameters: strike 313°; dip 70°; rake-115° with different depth (33 km).

Fig. 8 shows that the Coulomb stress changes are associated with the mainshock on the NW-SE striking fault plane of the M_w6.2 earthquake on November 25, 2000. The main event increased the Coulomb stress by about 1.0 bars in the region. Fig. 6(A) shows the Coulomb stress changes caused by the mainshock on the fault plane correlated with the second event which increased static stress mainly in the SE–NW of the seismogenic area.

In the case of an optimum thrust faulting (Fig. 8(C)), the lobed models of stress change using regional stress adjustment cover large zones of positive change that dominated landward and offshore of the main rupture and some regions of negative stress changes in the NE direction in offshore. Fig. 8(B) shows the cumulative Coulomb stress variations created on the fault plane of the second earthquake of November 25. The first vertical cross-section (A-B) confirms that the fault plane is associated with the first case and the second cross-section (A′-B′) shows that the fault plane is associated with the second earthquake. In both cases, we computed the static stress on a horizontal plane and a vertical cross-section (A-B, A′-B′) perpendicular to the fault strike of event. The vertical cross-sections give us sufficient information about the state of stress in normal faulting conditions in Fig. 9 (bottom). The comparison stress variations between the two cases are also clear at depth (Fig. 9). While the study of the stress induced on a cross-section (Fig. 9, bottom) indicates that the Coulomb stress increase in the area where aftershocks were located with a different depth. Remarkable

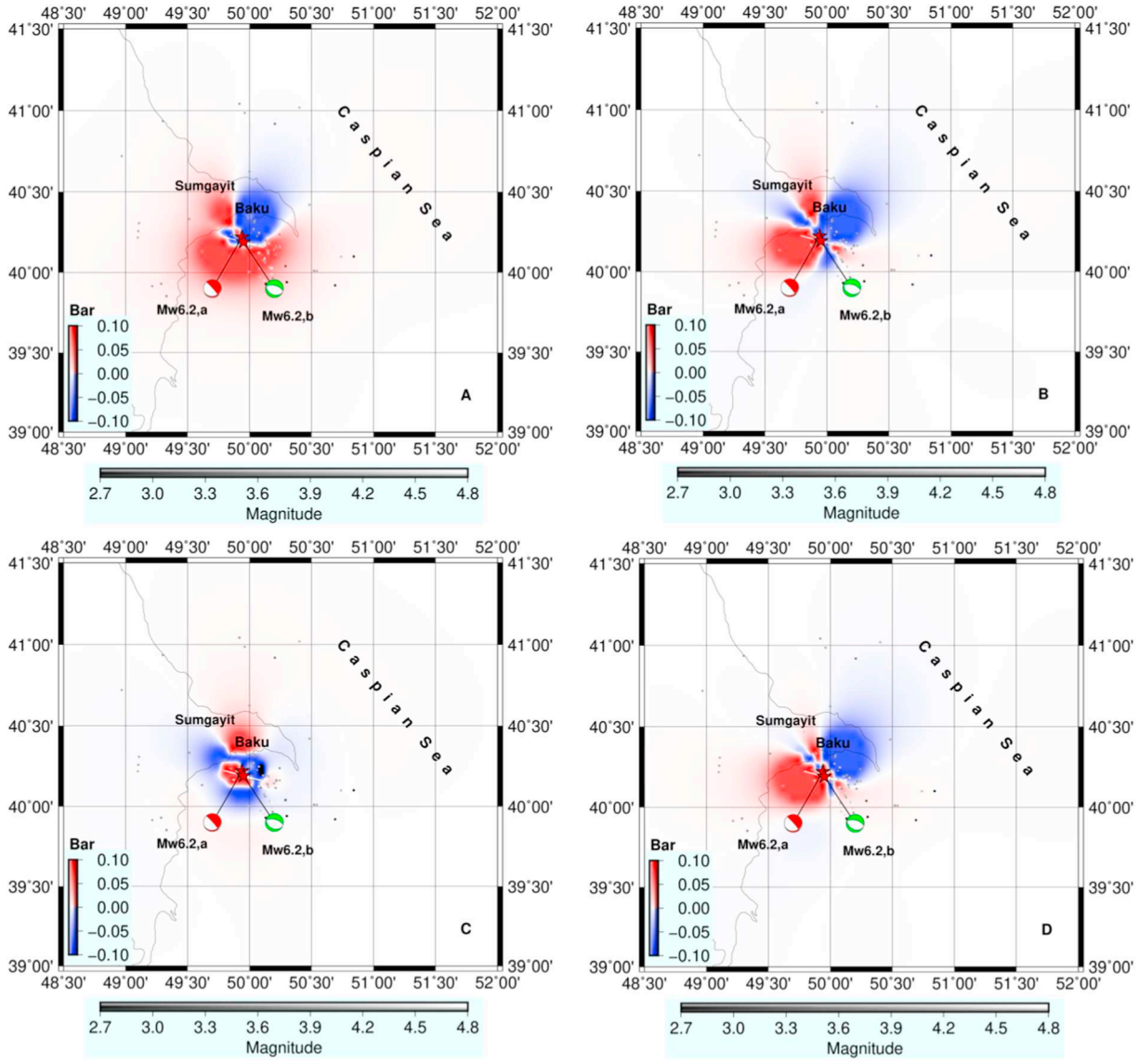

Fig. 8. Maps of Coulomb stress changes caused by the 2000 Baku earthquake calculated over the specific receiver fault (A) strike 318°; dip 85°; rake −77° and optimally oriented (B) strike-slip faulting (C) thrust faulting and (D) normal faulting. The grey dots denote the epicenters of the M ≥ 2.7 aftershocks (ISC, 2000/11/25–2002/11/25). Red focal mechanisms represent specific receiver fault is used for calculation. (For interpretation of the references to color in this figure legend, the reader is referred to the web version of this article.)

hypocenters fall in the region of positive stress changes and some hypocenters in the stress shadow of the 2000 earthquake. This error might come from several factors: either the hypocenter locations or possible factor is the higher pore pressure in this area.

The aftershocks are not uniformly distributed around the mainshock. Seventy-three aftershocks are caused within two years after the mainshock. More significant aftershocks are mainly distributed in the positive stress area in the southeast segment of the fault plane. Although three lower aftershocks are observed in the shadow of positive stress. The positive stress lobe on the fault tips is more extensive than the aftershock clusters. This may be according to the uncertainty of the parameters such as aftershocks location, stress magnitude and fault geometry. The depth of earthquakes has a significant influence on the Coulomb failure stress of thrust earthquakes (Lin and Stein, 2004). As shown in Fig. 9, the spatial distribution of Coulomb stress produced by the Baku earthquake shows that some of the aftershocks are not triggered by the mainshock. Through the statistics of the stress change pattern with aftershocks, most of the events are found in the regions where the stress change is positive.

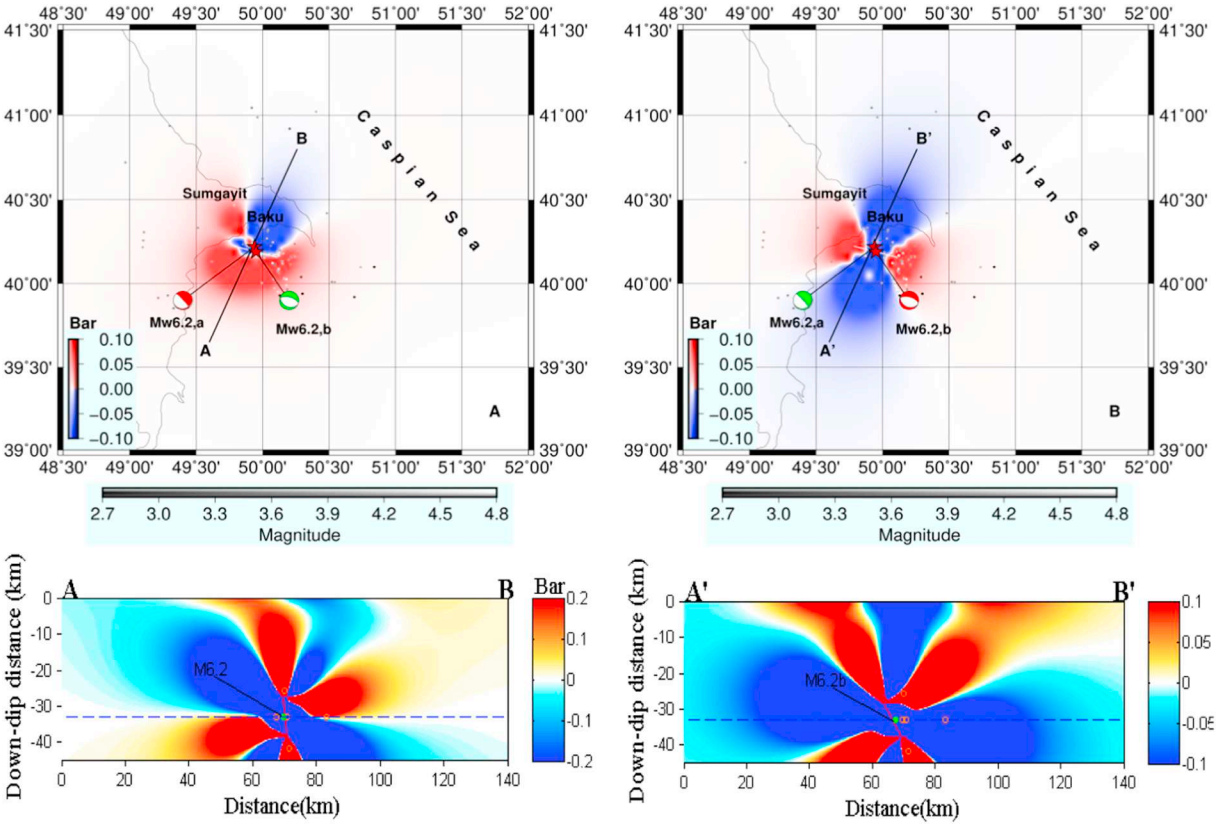

Fig. 9. Coulomb stress changes calculated for the first and second events. Vertical cross-sections oriented perpendicular to the strike of the fault modelled during the 2000 Baku earthquake along lines P1 (A-B) in panel A and P2 (A′-B′) in panel B, respectively.

4.5. Seismicity rate

We used the data from the ISC for 15 years after the mainshocks to constrain the seismicity rate changes (Fig. 10). The seismicity rate differences are calculated using the events after the mainshock and correlate them with the estimated Coulomb stress changes. Our results show that stress changes cause a meaningful variation in areas with high seismicity. The Coulomb stress decreases in around the main rupture of the Spitak earthquake, but the seismicity rate significantly increases. The contradiction is caused by the probable effect of aftershocks due to dynamic stress triggering. We find that the Coulomb stress decreases, and the seismicity also decreases in the north part of the Racha earthquake. The northeastern part of rupture is observed with increasing seismicity rate where Coulomb stress increase. In addition to static stress changes, the increased seismicity is connected with other factors, such as the stress or impact of other earthquakes. The high seismicity rate is estimated around the Baku earthquake. Positive Coulomb stress areas correlate with recent seismicity, implying that the Coulomb stress still influences recent seismicity. However, no significant effect between recent seismicity and the negative Coulomb stress areas are observed in the north of the source region of the 2000 Baku earthquake. In the future, we try to get more dense data to estimate larger area and compare with the Coulomb stress shadow areas.

5. Conclusion

Coulomb stress changes of the Racha (M_w6.9), Spitak (M_w6.8) and Baku (M_w6.2) earthquakes are investigated using available data related to the aftershock seismicity and the spatial correspondence between the recent seismicity rate and Coulomb stress are examined. Our results show that the recent seismicity rate is probably still affected by several large earthquakes. Stress changes make a significant difference in the region with relatively high seismicity rate. As interpreted from the stress change maps shown, there is a correspondence between the stress perturbations caused by the mainshocks and the observed spatial pattern of the aftershock distribution, indicating that Coulomb stress change modelling is a tool for aftershock hazard evaluation, especially for the mainshocks with long and damaging aftershock activity. The stress reductions of the earthquake and the triggering delay times are small with respect to the recurrence time of the earthquakes. The modelling proves that small stress increases (a few bars) may promote the existence of earthquakes. This effect indicates that strong earthquakes are resulted from a heterogeneous process that gradually produces the brittle crust, where future shocks occur. The spatial redistribution and increase of static stress caused by a strong earthquake may bring up a rupture on nearby faults that are close to this failure threshold.

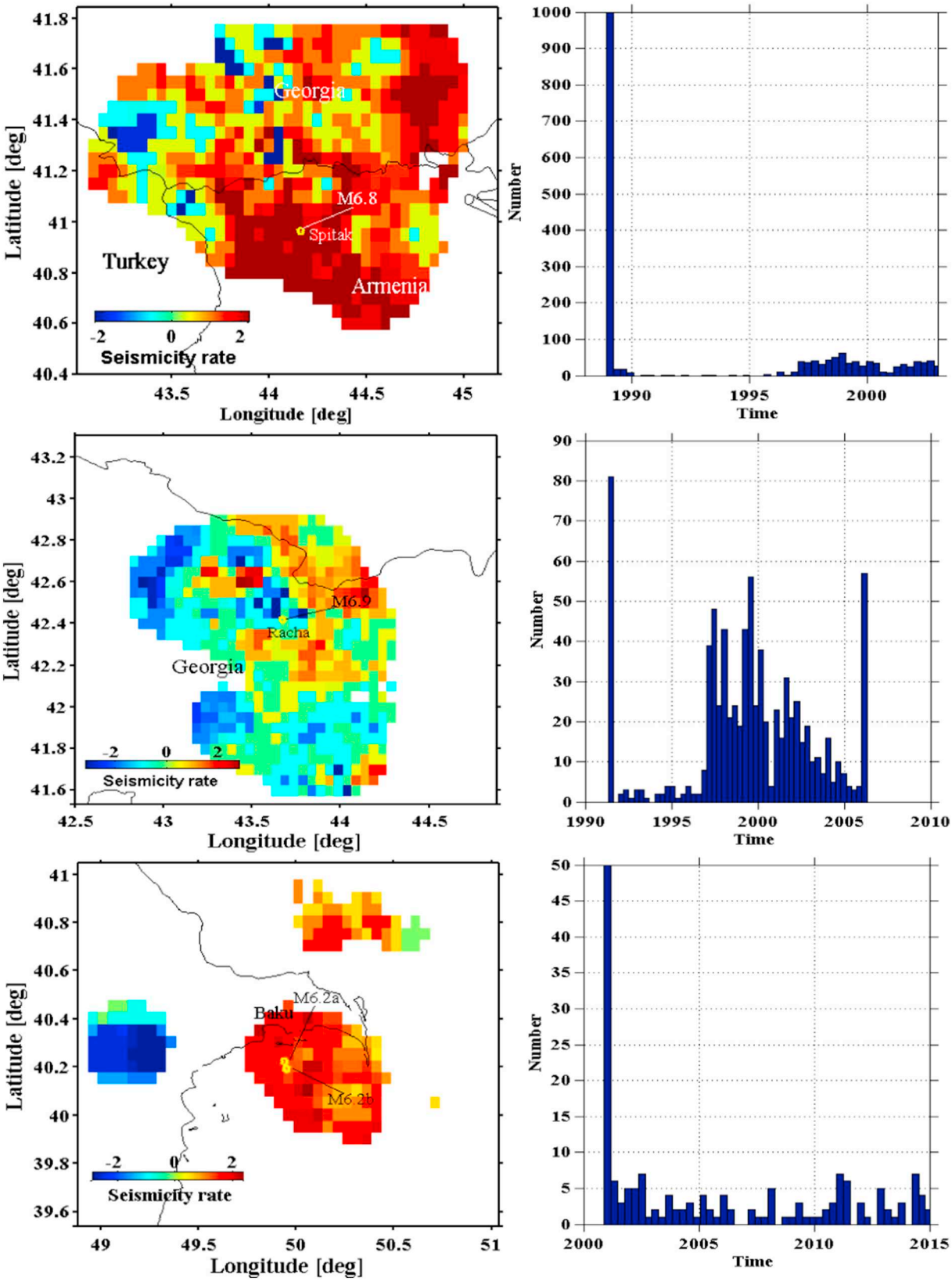

Fig. 10. The map shows the seismicity rate changes after the mainshocks. The seismicity rate is calculated with a radius of 20 km by 0.05° × 0.05° grid node. The positive and the negative values indicate increases and decreases of the seismicity rate.

Declaration of competing interests

The authors declare that they have no known competing financial interests or personal relationships that could have appeared to influence the work reported in this paper.

Acknowledgement

We are grateful to thank the Editor and two anonymous reviewers for their helpful comments and suggestions. All the maps are drawn using Generic Mapping Tools (GMT, www.soest.hawaii.edu/gmt) (Wessel et al., 2013) and some of the graphs are plotted using ZMAP (Wiemer, 2001). This work was supported by the National Key Research and Development Program of China Project (Grant No. 2018YFC0603502).

Appendix A. Supplementary data

Supplementary data to this article can be found online at https://doi.org/10.1016/j.pepi.2019.106326.

References

Ahadov, B., Jin, S., 2017. Present-day kinematics in the Eastern Mediterranean and Caucasus from dense GPS observations. Phys. Earth Planet. Inter. 268, 54–64.
Allen, M.B.S., Jones, A., Ismail-Zadeh, M.S., Anderson, L., 2002. Onset of subduction as the cause of rapid Pliocene-Quaternary subsidence in the South Caspian basin. Geology 30, 775–778.
Barazangi, M., Sandvol, E., Seber, D., 2006. Structure and tectonic evolution of the Anatolian plateau in eastern Turkey. SPECIAL PAPERS-GEOLOGICAL SOCIETY OF AMERICA 409, 463.
Çakir, Z., BARKA, A.A., Evren, E., 2003. Coulomb stress interactions and the 1999 Marmara earthquakes. Turk. J. Earth Sci. 12, 91–103.
Copley, A., Jackson, J., 2006. Active tectonics of the Turkish-Iranian plateau. Tectonics 25.
Ekström, G., Nettles, M., Dziewoński, A., 2012. The global CMT project 2004–2010: centroid-moment tensors for 13,017 earthquakes. Phys. Earth Planet. Inter. 200, 1–9.
Gephart, J.W., Forsyth, D.W., 1984. An improved method for determining the regional stress tensor using earthquake focal mechanism data: application to the San Fernando earthquake sequence. Journal of Geophysical Research: Solid Earth 89, 9305–9320.
Hardebeck, J., 1998. The static stress change triggering model: constraints from two southern California aftershock sequences. Journal of Geophysical Research: Solid Earth 103, 24427–24437. https://doi.org/10.1029/98JB00573.
Ishibe, T., Shimazaki, K., Satake, K., Tsuruoka, H., 2011. Change in seismicity beneath the Tokyo metropolitan area due to the 2011 off the Pacific coast of Tohoku earthquake. Earth Planets Space 63, 731–735.
Ishibe, T., Satake, K., Sakai, S., Shimazaki, K., Tsuruoka, H., Yokota, Y., Nakagawa, S., Hirata, N., 2015. Correlation between coulomb stress imparted by the 2011 Tohoku-Oki earthquake and seismicity rate change in Kanto. Japan, Geophysical Journal International. 201, 112–134. https://doi.org/10.1093/gji/ggv001.
Jackson, J., Priestley, K., Allen, M., Berberian, M., 2002. Active tectonics of the south Caspian basin. Geophys. J. Int. 148, 214–245.
Kadirov, F.A., Guliyev, I.S., Feyzullayev, A.A., Safarov, R.T., Mammadov, S.K., Babayev, G.R., Rashidov, T.M., 2014. GPS-based crustal deformations in Azerbaijan and their influence on seismicity and mud volcanism. Izvestiya, Physics of the Solid Earth 50 (6), 814–823.
King, G.C., Stein, R.S., Lin, J., 1994. Static stress changes and the triggering of earthquakes. Bull. Seismol. Soc. Am. 84, 935–953.
Lin, J., Stein, R.S., 2004. Stress triggering in thrust and subduction earthquakes and stress interaction between the southern San Andreas and nearby thrust and strike-slip faults. Journal of Geophysical Research: Solid Earth 109.
McCloskey, J., Nalbant, S.S., 2009. Near-real-time aftershock hazard maps. Nat. Geosci. 2, 154.
McKenzie, D., 1970. Plate tectonics of the Mediterranean region. Nature 226, 239–243.
Michael, A.J., 1984. Determination of stress from slip data: faults and folds. Journal of Geophysical Research: Solid Earth 89, 11517–11526.
Nalbant, S.S., McCloskey, J., Steacy, S., Barka, A.A., 2002. Stress accumulation and increased seismic risk in eastern Turkey. Earth Planet. Sci. Lett. 195, 291–298.
Pacheco, J., Estabrook, C., Simpson, D., Nábělek, J., 1989. Teleseismic body wave analysis of the 1988 Armenian earthquake. Geophys. Res. Lett. 16, 1425–1428.
Parsons, T., 2005. Significance of stress transfer in time-dependent earthquake probability calculations. Journal of Geophysical Research: Solid Earth 110.
Parsons, T., Stein, R.S., Simpson, R.W., Reasenberg, P.A., 1999. Stress sensitivity of fault seismicity: a comparison between limited-offset oblique and major strike-slip faults. Journal of Geophysical Research: Solid Earth 104, 20183–20202.
Philip, H., Cisternas, A., Gvishiani, A., Gorshkov, A., 1989. The Caucasus: an actual example of the initial stages of continental collision. Tectonophysics 161, 1–21.
Reasenberg, P.A., Simpson, R.W., 1992. Response of regional seismicity to the static stress change produced by the Loma Prieta earthquake. Science 255, 1687–1690.
Reilinger, R., McClusky, S., Vernant, P., Lawrence, S., Ergintav, S., Cakmak, R., Ozener, H., Kadirov, F., Guliev, I., Stepanyan, R., 2006. GPS constraints on continental deformation in the Africa-Arabia-Eurasia continental collision zone and implications for the dynamics of plate interactions. Journal of Geophysical Research: Solid Earth 111.
Roeloffs, E.A., 1988. Hydrologic precursors to earthquakes: a review. Pure Appl. Geophys. 126, 177–209.
Steacy, S., Marsan, D., Nalbant, S.S., McCloskey, J., 2004. Sensitivity of static stress calculations to the earthquake slip distribution. Journal of Geophysical Research: Solid Earth 109.
Stein, R.S., Barka, A.A., Dieterich, J.H., 1997. Progressive failure on the North Anatolian fault since 1939 by earthquake stress triggering. Geophys. J. Int. 128, 594–604.
Tan, O., Taymaz, T., 2006. Active tectonics of the Caucasus: earthquake source mechanisms and rupture histories obtained from inversion of teleseismic body waveforms. SPECIAL PAPERS-GEOLOGICAL SOCIETY OF AMERICA 409, 531.
Toda, S., 2008. Coulomb stresses imparted by the 25 March 2007 Mw = 6.6 Noto-Hanto, Japan, earthquake explain it's 'butterfly' distribution of aftershocks and suggest a heightened seismic hazard. Earth Planets Space 60, 1041–1046.
Toda, S., Stein, R., 2003. Toggling of seismicity by the 1997 Kagoshima earthquake couplet: a demonstration of time-dependent stress transfer. Journal of Geophysical Research: Solid Earth 108.
Toda, S., Stein, R.S., Richards-Dinger, K., Bozkurt, S.B., 2005. Forecasting the evolution of seismicity in southern California: animations built on earthquake stress transfer. Journal of Geophysical Research: Solid Earth 110.
Triep, E., Abers, G., Lerner-Lam, A.L., Mishatkin, V., Zakharchenko, N., Starovoit, O., 1995. Active thrust front of the Greater Caucasus: the April 29, 1991, Racha earthquake sequence and its tectonic implications. Journal of Geophysical Research: Solid Earth 100, 4011–4033.
Tseng, T.-L., Hsu, H.-C., Jian, P.-R., Huang, B.-S., Hu, J.-C., Chung, S.-L., 2016. Focal mechanisms and stress variations in the Caucasus and northeast Turkey from constraints of regional waveforms. Tectonophysics 691, 362–374.
Wells, D.L., Coppersmith, K.J., 1994. New empirical relationships among magnitude, rupture length, rupture width, rupture area, and surface displacement. Bull. Seismol. Soc. Am. 84, 974–1002.
Wessel, P., et al., 2013. Generic mapping tools: improved version released. Eos, Transactions American Geophysical Union 94, 409–410. https://doi.org/10.1002/2013EO450001.
Wiemer, S., 2001. A software package to analyze seismicity: ZMAP. Seismol. Res. Lett. 72, 373–382.